Astron. Astrophys. 244, 84–94 (1991)

ASTRONOMY AND ASTROPHYSICS

V 645 Cygni: a decelerating molecular outflow?

L. Verdes-Montenegro [1], J. F. Gómez [1], J. M. Torrelles [1], G. Anglada [2,⋆], R. Estalella [2,⋆], and R. López [2,⋆]

[1] Instituto de Astrofísica de Andalucía, Apdo. Correos 2144, E-18080 Granada, Spain
[2] Departament d'Astronomia i Meteorologia, Universitat de Barcelona, Av. Diagonal 647, E-08028 Barcelona, Spain

Received May 25, accepted August 30, 1990

Abstract. V 645 Cygni (AFGL 2789) is a young stellar object associated with a bipolar molecular outflow with a modest degree of collimation. In this paper we present IRAM 30-m observations of the CO ($J=2\rightarrow1$), ^{13}CO ($J=1\rightarrow0$) and C^{18}O ($J=1\rightarrow0$) rotational transition lines toward this region. At relatively low velocities the molecular outflow presents a bipolarity in the north-south direction, with the red and blueshifted CO lobes separated by $\sim20''$. This angular separation decreases as the velocity increases. At higher velocities the outflow appears isotropic. The physical parameters obtained for the V 645 Cyg molecular outflow (i.e., mass, momentum rate and mechanical luminosity) are much lower than the parameters derived for other outflows with exciting sources of similar luminosities ($L_*\simeq10^4\ L_\odot$). In particular, this result makes it possible that radiation pressure may be responsible for generating the stellar wind associated with V 645 Cyg. All these results lead us to suggest that the outflowing molecular gas could be decelerating as it moves away from the central V 645 Cyg position.

The integrated C^{18}O emission presents an elongated structure with a velocity gradient of $\sim0.7\,\mathrm{km\,s^{-1}\,pc^{-1}}$ in the east-west direction. The mass derived is sufficient to bind these motions.

Key words: interstellar medium: molecules – stars: formation, mass loss

1. Introduction

The mass ejection constitutes an important stage of the stellar evolution (see, e.g., Rodríguez et al. 1982). In general, molecular outflows show a bipolar geometry; that is, the blue and red emission lobes are spatially separated. Only a small fraction of the observed outflows present a monopolar or isotropic geometry. However, it is possible that some actual bipolar outflows look isotropic due to a combination of the alignment of their axes with the line of sight and the lack of enough angular resolution in the observations. For these reasons, high-angular resolution observations of the molecular gas can give us new information on the morphology and collimation processes of bipolar outflows with an apparent low degree of collimation. This is the case of V 645 Cygni (AFGL 2789).

Send offprint requests to: L. Verdes-Montenegro

⋆ Laboratori d'Astrofísica, Societat Catalana de Física (IEC)

V 645 Cyg is a young stellar object associated with an extended optical nebulosity. Cohen (1977) found three optical knots, N0, N1, and N2, which he interpreted as reflection nebulae illuminated by the young stellar object. In addition, Goodrich (1986) found that the reflection nebula has a *"duck-like"* shape with a long *"beak"* and an HH object to the south of it. Furthermore, the *"beak"*, the brightest knot N0, and the HH object are aligned in the north-south direction, suggesting an optical outflow. The location of the exciting source is very close ($\lesssim5''$) to N0 (Lenzen 1987; Hamann & Persson 1989). H_2O maser emission (Lada et al. 1981) and an unusual OH maser with several velocity components (Morris & Kazès 1982), are related to V 645 Cyg. Goodrich (1986) gives a stellar luminosity $L_*=6\ 10^4\ L_\odot$ for V 645 Cyg, assuming a distance of 3.5 kpc. This is the distance adopted in the present paper.

Curiel et al. (1989) detected an extended ($\sim5''$) radio source spatially coincident with the core source. These authors suggest that the ionized gas is produced by the shock of a neutral stellar wind with the surrounding molecular gas. We must note that this radio continuum emission could be related with the V 645 Cyg/HH object. If this is true, it would be another case where radio continuum emission is detected toward an HH object associated with a high-luminosity ($L\geq10^3\ L_\odot$) young star (see Rodríguez 1989; Torrelles 1990).

V 645 Cyg has associated a bipolar molecular outflow with a modest degree of collimation. CO ($J=1\rightarrow0$) observations (beam size $\simeq1'.1$) carried out by Rodríguez et al. (1981) revealed the presence of CO high-velocity wings, with the blue and redshifted emissions spatially coincident. Further CO ($J=2\rightarrow1$) observations (beam size $\simeq30''$) by Torrelles et al. (1987) showed that the molecular outflow is bipolar. At small scales ($\sim15''$) the outflow is collimated in the north-south direction, coinciding with the direction of the optical outflow observed by Goodrich (1986), while at larger scales ($\geq1'$) the CO outflow is reoriented into a southeast-northwest direction. CO ($J=3\rightarrow2$) observations (beam size $\simeq26''$) by Schulz et al. (1989) revealed the bipolarity of the molecular outflow in the southeast-northwest direction. Goodrich (1986) and Torrelles et al. (1987) suggested the presence of a *"warped"* disk in order to explain the change of orientation of the outflow axis from scales of $\sim15''$ to $\sim1'$. Ammonia observations carried out by Torrelles et al. (1983, 1989) with the 37-m Haystack telescope (beam size $\simeq1'.4$) and the VLA system in the D configuration (beam size $\simeq14''$) show a condensation elongated in the northeast-southwest direction, perpendicular to the outflow axis at scales of $\sim1'$. The VLA ammonia observations indicate that the high density gas found at scales of $\sim14''$ does not play (at

these scales) an important role in the collimation process of the north-south bipolar CO outflow since V645 Cyg is located at the edge of the VLA-NH_3 condensation.

In this paper we present IRAM 30-m observations of the CO ($J=2\rightarrow1$), ^{13}CO ($J=1\rightarrow0$) and C^{18}O ($J=1\rightarrow0$) rotational transition lines toward V645 Cyg. The aim of these new observations is to improve the definition of the morphology of the molecular outflow near the activity center, as well as to study the morphology, kinematics and excitation of the ambient molecular cloud, and its possible role in the focusing mechanism of the outflow. We describe and present our observations in Sect. 2, in Sect. 3 we discuss the results, and finally in Sect. 4, we give a summary of our main conclusions.

2. Observations

2.1. System parameters

The observations of the CO ($J=2\rightarrow1$), ^{13}CO ($J=1\rightarrow0$), and C^{18}O ($J=1\rightarrow0$) rotational transition lines were carried out in February 1988 with the 30-m telescope of the Institut de Radio Astronomie Millimétrique (IRAM) at Pico Veleta (Granada, Spain). These three rotational transition lines were observed simultaneously by using two SIS receivers and two filter banks, one of 512×1 MHz channels (velocity resolution $\simeq1.3$ km s^{-1} at $\lambda\simeq1.3$ mm) and the other one of 256×100 kHz channels (velocity resolution $\simeq0.3$ km s^{-1} at $\lambda\simeq2.7$ mm) split in two halves in order to observe the ^{13}CO and C^{18}O lines. At the observing wavelengths of $\lambda\simeq1.3$ mm (CO) and $\lambda\simeq2.7$ mm (^{13}CO, C^{18}O) the beam sizes were $\sim13''$ and $22''$, respectively. From observations of unresolved sources the rms pointing error of the telescope was found to be lower than $2''$. The observations were made using the position switching mode. Temperatures in this paper are given in a T_R^* scale (Kutner & Ulich 1981). System temperatures were typically ~450 K.

Our maps were centered on the position of knot N0, that is, $\alpha(1950)=21^h38^m10^s.6$, $\delta(1950)=50°00'43''$. Offset positions given in this paper are relative to this central position. Typical one sigma sensitivities per channel for the three observed lines were ~0.03 K (CO), ~0.10 K (^{13}CO), and ~0.20 K (C^{18}O). In a few positions, the observed C^{18}O spectra have not been used in our analysis due to the presence of ripples in their baselines. In Table 1 we give the line parameters obtained from Gaussian fits to the observed spectra at the central position.

2.2. CO ($J=2\rightarrow1$) data: the molecular outflow

In Fig. 1 we show the CO spectrum obtained toward the V645 Cyg central position. The maximum of the CO line intensity is at $\sim9''$ northwest of the central position, with a value of $T_R^*(\mathrm{CO})=13.3$ K at $V_{LSR}=-44$ km s^{-1}. Assuming a filling factor of one, we estimate a kinetic temperature of ~19 K for the molecular gas. The CO line width at half maximum (ΔV) increases toward the central region, reaching a maximum value $\Delta V(\mathrm{CO})=8.8$ km s^{-1} at $(-19''.5, -6''.5)$. We did not find any significant gradient in the velocity of the CO peak. High-velocity CO wings (see Fig. 1) are observed up to ~-64 km s^{-1} and ~-19 km s^{-1} for the blueshifted and redshifted emission, respectively. This range of velocities is wider than that detected by Torrelles et al. (1987), because of our higher signal-to-noise ratio.

Our CO observations reveal an interesting relationship between the spatial distribution of the outflowing gas and its velocity. A detailed analysis of the individual velocity channels shows that at relatively low velocities with respect to the velocity of the ambient molecular gas, taken as $V_{LSR}=-44$ km s^{-1}, the molecular outflow is bipolar in the north-south direction. In Fig. 2 we show the contour map of the T_R^*(CO) intensity at $V_{LSR}=-49.8$ km s^{-1} (blueshifted) and -38.1 km s^{-1} (redshifted). For these velocities the red and blueshifted CO lobes are clearly displaced in the north-south direction. At higher relative velocities the angular separation decreases and, in particular, the outflow appears isotropic at velocities $V_{LSR}=-59$ km s^{-1} and -29 km s^{-1}. This is illustrated in Fig. 3, where we show the half power contours of the red and the blueshifted CO lobes at selected velocities. In addition, in Fig. 4 we show the centroid positions (offset in the north-south direction, $\Delta\delta$) of the half power contours of the red and the blueshifted CO lobes as a function of velocity. By comparing pairs of points with symmetrical relative velocities with respect to $V_{LSR}=-44$ km s^{-1}, we see (Fig. 4) that the angular separation between the blue and the redshifted centroids decreases gradually as the relative velocity increases. The maximum observed separation is $20''$, for relative velocities of ±6 km s^{-1}.

Note that the redshifted emission is stronger than the blueshifted emission. This asymmetry can be understood as a result of radiative transfer effects in outflowing motions (Bally & Lada 1983; Cabrit & Bertout 1986; Anglada et al. 1987). As a consequence, we have estimated centroid positions up to higher relative velocities for the redshifted gas. At high relative velocities the redshifted centroids are displaced to the south of the central position, known with an uncertainty of $\sim5''$ (Hamann & Persson 1989). The maximum displacement is $\sim8''$, for the highest observed relative velocity of $+24$ km s^{-1}. Unfortunately, we are not able to make a reasonable comparison with the centroid position of the corresponding symmetrical blueshifted gas at relative velocity of -24 km s^{-1} since the wing emission is faint at this velocity. The fact that some redshifted centroids appear a few arcsec toward the south of the central position could be due to the low collimation of the outflow near V645 Cyg and to projection effects (see Sect. 3).

When we integrate the high-velocity CO wings over a wide range of velocities ($-69\leq V_{LSR}\leq-50$ km s^{-1}, blueshifted CO; $-38\leq V_{LSR}\leq-19$ km s^{-1}, redshifted CO; Fig. 5), the outflow seems to be isotropic, except for the lower integrated intensity contours, which still display a bipolar geometry in the north-south direction. This is because of the blending of the bipolar distribution (at lower velocities) with the isotropic distribution (at higher velocities).

The parameters of the V645 Cyg outflow, such as integrated intensity, opacity, column densities, size, mass, momentum rate and mechanical luminosity, are presented in Table 2. These parameters have been calculated from the CO ($J=2\rightarrow1$) and the

Table 1. Line parameters[a]

Line	T_R^* (K)	ΔV (km s^{-1})	V_{LSR} (km s^{-1})
CO ($J=2\rightarrow1$)	13.1 ± 0.3	7.70 ± 0.02	-43.80 ± 0.01
^{13}CO ($J=1\rightarrow0$)	7.8 ± 0.1	2.51 ± 0.03	-43.88 ± 0.01
C^{18}O ($J=1\rightarrow0$)	1.5 ± 0.1	2.25 ± 0.15	-43.68 ± 0.05

[a] Obtained from Gaussian fits to the observed spectra at the central position [$\alpha(1950)=21^h38^m10^s.6$; $\delta(1950)=50°00'43''$].

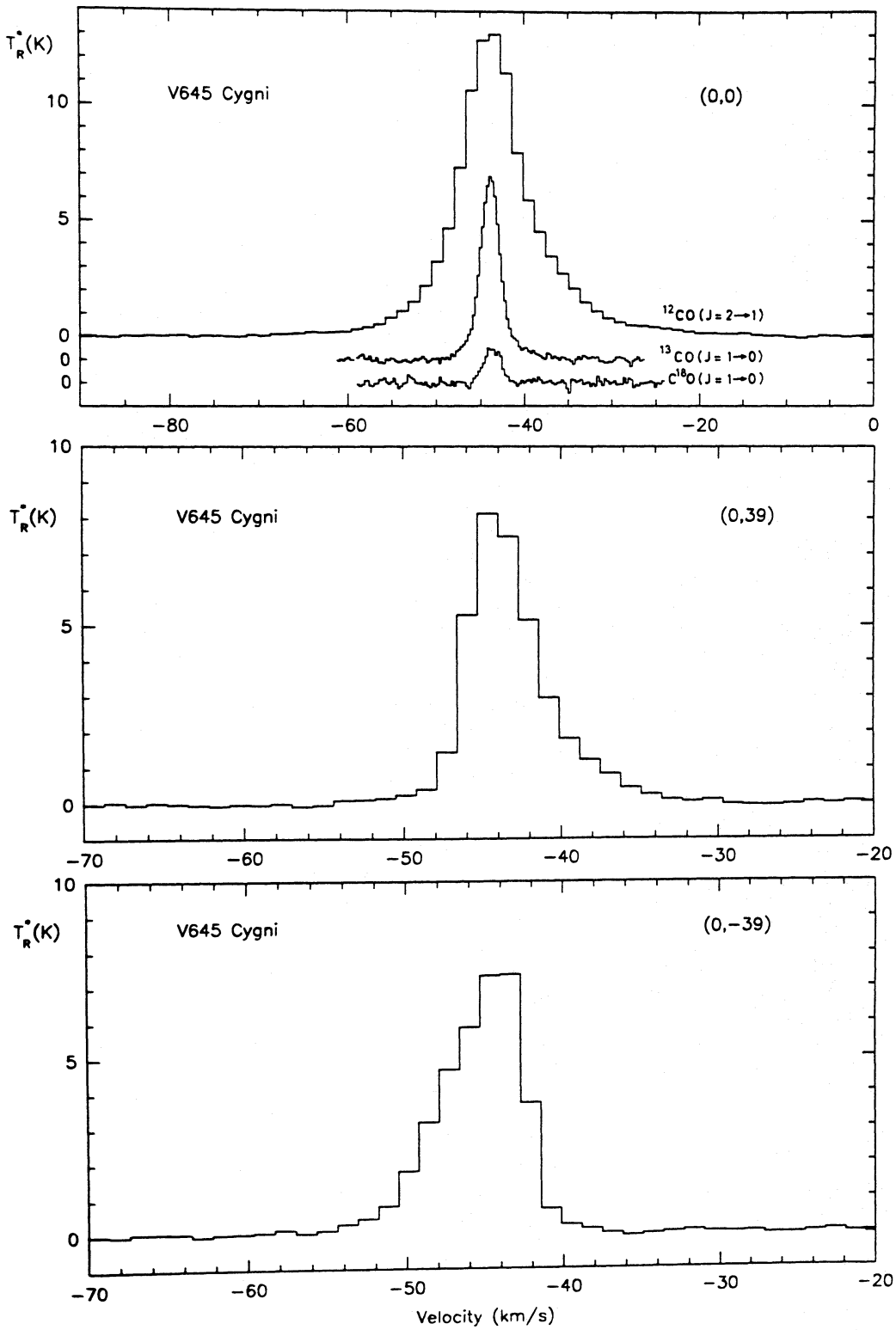

Fig. 1. Observed spectra of the CO ($J=2\rightarrow1$), ^{13}CO ($J-1\rightarrow0$), and C^{18}O ($J=1\rightarrow0$) rotational transition lines toward the V 645 Cyg positin $\alpha(1950)=21^{h}38^{m}10\overset{s}{.}6$ and $\delta(1950)=50°00'43''$, and observed CO ($J=2\rightarrow1$) spectra at selected positions. Offset positions are in arcsec

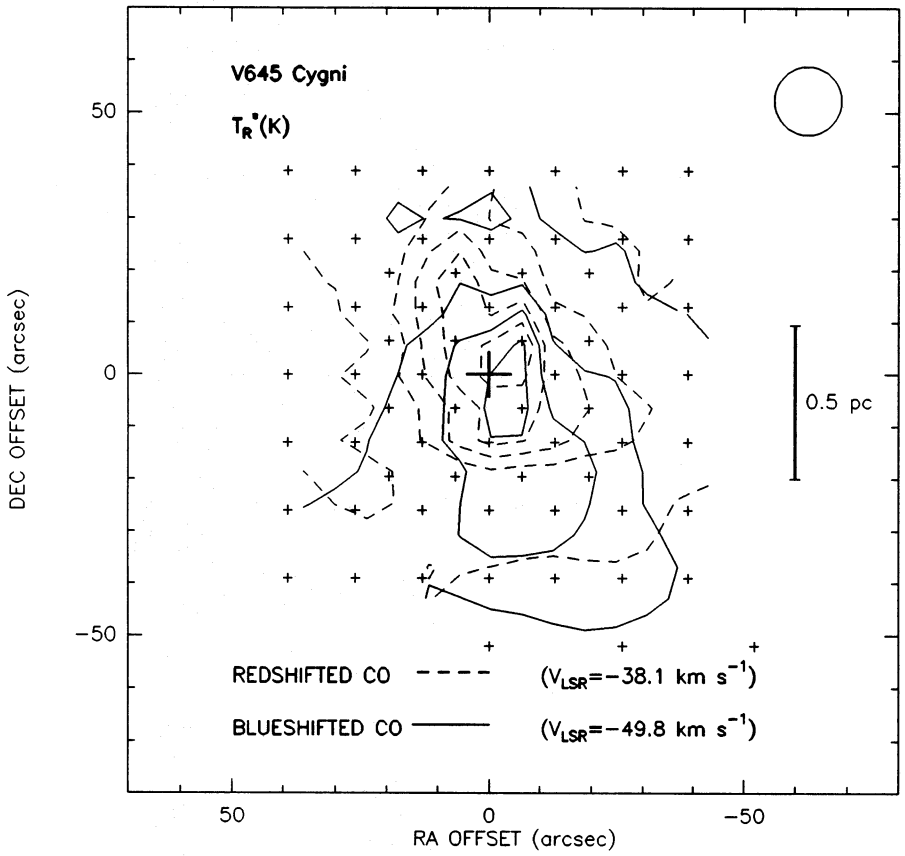

Fig. 2. Contour map of the CO ($J=2\rightarrow1$) line intensity at $-49.8\,\mathrm{km\,s^{-1}}$ (blueshifted CO) and $-38.1\,\mathrm{km\,s^{-1}}$ (redshifted CO). The lowest contour level is $T_R^*=0.2\,\mathrm{K}$, and the increment step is 1 K

^{13}CO ($J=1\rightarrow0$) data (see Sect. 2.3) following the procedures explained in the footnotes of that table.

We have not observed the bipolarity of the molecular outflow in the southeast-northwest direction reported by Torrelles et al. (1987) and Schulz et al. (1989) at larger scales ($\geq 1'$). This may be due to the fact that our higher angular resolution enhances the behavior of the molecular outflow at smaller scales and also to the fact that we have mapped a smaller region. In this sense, the ^{13}CO spectra observed at the south-east corner of our map show an increase of blueshifted emission (see Sect. 2.3) that could be related to the orientation of the molecular outflow in the southeast-northwest direction found at larger scales ($\geq 1'$). The fact that we do not observe the southeast-northwest bipolarity may cause that we are underestimating the outflow mass because we have not mapped far enough.

2.3. ^{13}CO ($J=1\rightarrow0$) and C^{18}O ($J=1\rightarrow0$) data: the ambient molecular cloud

Figure 1 shows the ^{13}CO and C^{18}O spectra obtained toward the (0,0) position. The ^{13}CO spectrum presents weak red and blue wings extending up to $V_{LSR}\simeq-48\,\mathrm{km\,s^{-1}}$ (blueshifted wing) and $V_{LSR}\simeq-39\,\mathrm{km\,s^{-1}}$ (redshifted wing) at a level $T_R^*(^{13}\mathrm{CO})\simeq0.3\,\mathrm{K}$. In Fig. 6 we show the integrated intensity of the ^{13}CO wings over the ranges $-52\leq V_{LSR}\leq-46\,\mathrm{km\,s^{-1}}$ (blueshifted) and $-42\leq V_{LSR}\leq-36\,\mathrm{km\,s^{-1}}$ (redshifted). In the central part of the map, we observe a north-south bipolarity similar to that observed in CO at low relative velocities. Furthermore, there is a noticeable enhancement of the ^{13}CO blueshifted wings toward the southeast corner of the map (see also Fig. 7), suggesting an increase of blueshifted emission in that direction, outside the mapped region. We think that this high-velocity emission could be associated with the large scale molecular outflow in the southeast-northwest direction observed by Torrelles et al. (1987) and Schulz et al. (1989). No wings have been detected in the C^{18}O spectra.

In Fig. 8 we present a map of the integrated intensity of the ^{13}CO line over the range $-50\leq V_{LSR}\leq-38\,\mathrm{km\,s^{-1}}$. The contribution of the ^{13}CO line wings to this integration is negligible. The integrated ^{13}CO emission reaches a maximum value of $24.5\,\mathrm{K\,km\,s^{-1}}$ near V645 Cyg at (6″.5, 6″.5). Unfortunately, we can not discuss on the morphology of this structure since the ^{13}CO emission was not fully mapped toward the eastern region. However, in spite of this limitation, our ^{13}CO map is consistent with that obtained by Torrelles et al. (1987). The map of the integrated intensity of the C^{18}O line over the range $-50\leq V_{LSR}\leq-38\,\mathrm{km\,s^{-1}}$ is shown in Fig. 9. The C^{18}O structure is similar to that observed in ^{13}CO, but more elongated in the central region. Near V645 Cyg, for the high value contours ($\geq 2\,\mathrm{K\,km\,s^{-1}}$), the C^{18}O structure appears elongated in the east-west direction, but for the low value contours ($\leq 2\,\mathrm{K\,km\,s^{-1}}$) the structure bends toward the northeast direction. We must emphasize that the northeast-southwest orientation of the C^{18}O structure is not well determined, since our observations did not fully cover the north-east region. However, since this orientation was also found both in the ^{13}CO and NH_3 structures by Torrelles et al. (1987, 1989), we think that it is quite significant.

In Table 3 we list the parameters of the ambient molecular cloud traced by the ^{13}CO and C^{18}O lines: line intensities, opacities, integrated intensities, column densities, size, mass and visual extinction. These parameters were obtained as indicated in the

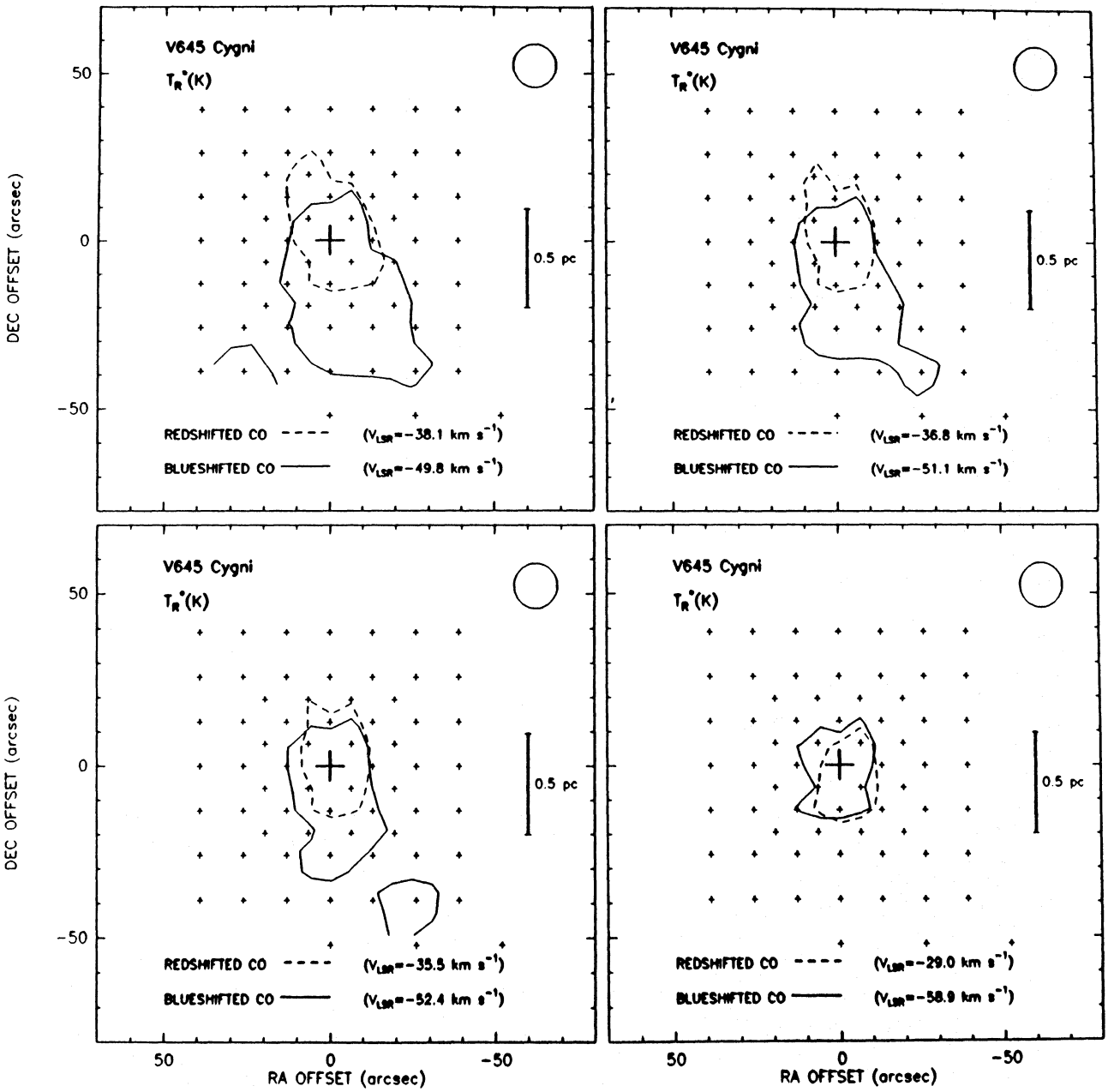

Fig. 3. Half intensity contours of the blueshifted and redshifted CO ($J=2\rightarrow1$) emission at selected velocities. Note that the angular separation between the red and blue CO lobes decreases as the velocity of the outflow relative to the ambient molecular cloud ($V_{LSR}=-44\,\mathrm{km\,s^{-1}}$) increases (see also Fig. 4)

footnotes of Table 3. We derive opacities $\tau_{13}\simeq0.7$ and $\tau_{18}\simeq0.09$, which imply an abundance $[^{13}CO/C^{18}O]\simeq8$. Given the spatial coincidence of the ^{13}CO and $C^{18}O$ emission and the low opacity of the $C^{18}O$ emission, we have used this last molecule to estimate the mass of the ambient molecular condensation, $\geq140\,M_\odot$. This value is a lower limit as our map is unfinished toward the north-east region.

In Fig. 10 we show ^{13}CO and $C^{18}O$ position-velocity diagrams along the north-south and east-west directions across the central position. We observe a velocity gradient along the east-west direction, with similar values of $\sim0.5\,\mathrm{km\,s^{-1}\,pc^{-1}}$ and $\sim0.7\,\mathrm{km\,s^{-1}\,pc^{-1}}$ for the ^{13}CO and $C^{18}O$ emission, respectively. Velocity gradients are not evident in the north-south position-velocity diagrams. There is also a broadening of the $C^{18}O$ line width toward the central region, with a line full width at half maximum $\Delta V(C^{18}O)\simeq2.3\,\mathrm{km\,s^{-1}}$. This line width decreases to $\sim1.6\,\mathrm{km\,s^{-1}}$ for an angular distance of $\sim30''$ from the central position (see Fig. 10).

3. Discussion

The estimated parameters for the V645 Cyg molecular outflow, i.e., mass, momentum rate, and mechanical luminosity (Table 2), are much lower than the derived parameters for other outflows with exciting sources of similar luminosities, $L_*\simeq10^4\,L_\odot$ (see

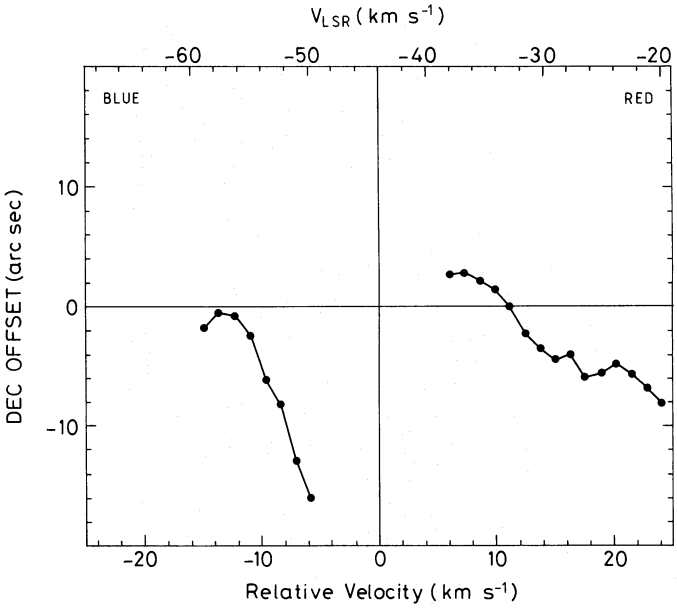

Fig. 4. Centroid position of the half intensity contours of the CO ($J=2\rightarrow1$) high velocity emission as a function of velocity. The declination offsets are relative to the assumed position of the exciting source (coordinates given in Fig. 1). The blueshifted lobes follow a power law given by $[V/\mathrm{km\,s^{-1}}] \simeq 13\times[|\Delta\delta|/\mathrm{arcsec}]^{-0.2}$, where V is the blueshifted centroid relative velocity. Position errors are lower than 2″

Rodríguez et al. 1982 and Lada 1985 for reviews of outflows). In fact, for the majority of the sources the derived momentum rate in the outflow ($\dot{P}$) is several orders of magnitude larger than the derived momentum rate in the radiation field (L_*/c) of the powering star. This is at the origin of the so-called *"momentum problem"* (see, e.g., Dyson, 1984) in the case that molecular outflows are momentum driven by stellar winds. V645 Cyg does not seem to have this problem since the derived momentum rate in the molecular outflow, $\sim 10^{-3}\ M_\odot\,\mathrm{km\,s^{-1}\,yr^{-1}}$ (Table 2), is similar to the momentum rate in the radiation field, $L_*/c \simeq 10^{-3}\ M_\odot\,\mathrm{km\,s^{-1}\,yr^{-1}}$ (for $L_* = 6\ 10^4\ L_\odot$; Goodrich 1986). In spite of the uncertainties in the derived parameters of the outflow, mainly introduced by uncertainties in distance, abundance, angle of view, velocity range of integration for the high-velocity wings and assumption of filling factor of one, we think that this result may imply that the stellar wind related to V645 Cyg can be generated by a *classical* mechanism such as radiation pressure.

One of the most relevant aspects related to bipolar outflows is their kinematics. Ascertaining, for example, whether the gas is accelerated or decelerated as it moves away from the powering source is an important clue to understand the origin of outflows. In particular, molecular outflows with an accelerating pattern, i.e., observed velocities increasing outward from the powering source, may in principle be explained by: (1) magneto-hydrodynamic winds arising from rotating magnetic disks and accelerating out to the Alfvén surface (Uchida & Shibata 1985; Pudritz & Norman 1986), (2) explosive outflows (FU Orionis events), and (3) latitude-dependent winds (Herbig 1968;

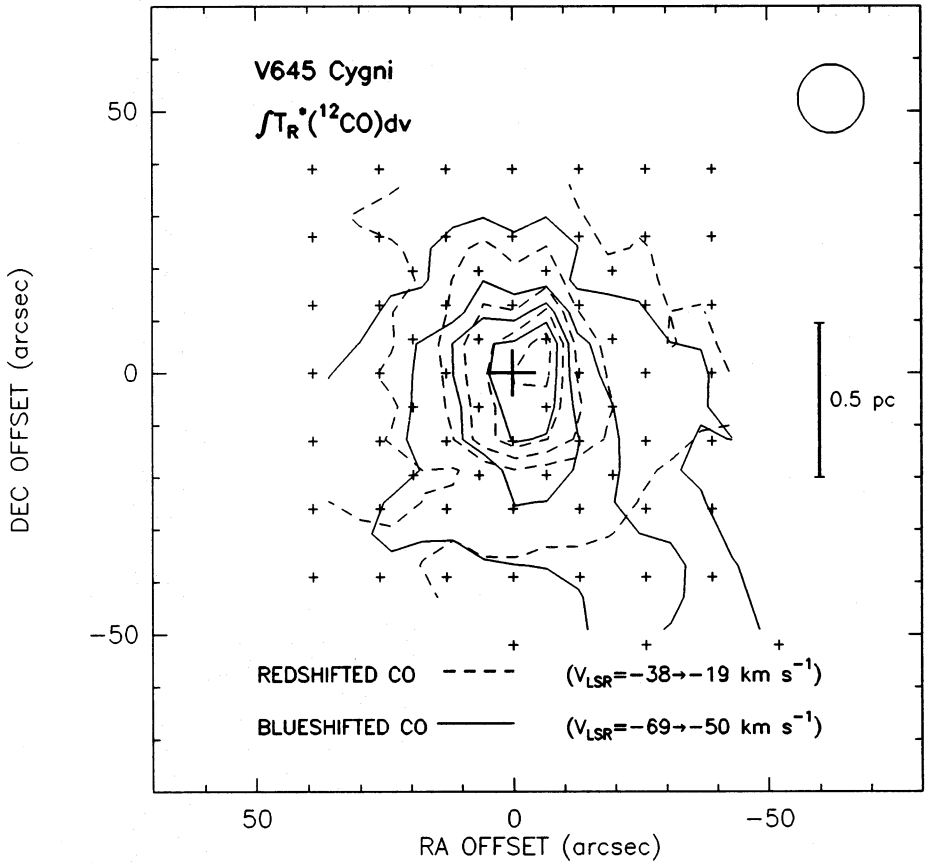

Fig. 5 Contour map of the integrated intensity of the CO ($J=2\rightarrow1$) line wings over a velocity ranges from -69 to $-50\,\mathrm{km\,s^{-1}}$ (blueshifted gas) and from -38 to $-19\,\mathrm{km\,s^{-1}}$ (redshifted gas). Contour levels are 1, 4, 7 and 10 K km s^{-1} (blueshifted emission), and 1, 6, 11, 16, and 21 K km s^{-1} (redshifted emission)

Table 2. Outflow parameters[a]

(V_{min}, V_{max})[b] (km s^{-1})	$\int T_R^*(CO, ^{13}CO)\,dv$[c] (K km s^{-1})	τ[d]	$N(CO, ^{13}CO)$[e] (10^{15} cm^{-2})	$N(H_2)$[f] (10^{19} cm^{-2})	$l_a \times l_b$[g] (pc)	M[h] ($M_\odot$)	$\dot{P}$[i] ($M_\odot$ km s^{-1} yr^{-1})	L_{mech}[j] ($L_\odot$)
CO (−69, −50)	12.9	0.5	7.7	4	0.6 × 0.4	0.1	$8\ 10^{-5}$	0.1
^{13}CO (−50, −46)	2.7	0.1	3.4	170	0.4 × 0.4	3.4	$3\ 10^{-4}$	0.1
^{13}CO (−42, −38)	3.0	0.1	3.8	190	0.5 × 0.4	4.8	$4\ 10^{-4}$	0.2
CO (−38, −19)	23.1	0.4	14.4	8	0.5 × 0.3	0.2	$3\ 10^{-4}$	0.7

[a] The outflow parameters have been obtained from integration of the ^{13}CO ($J = 1 \rightarrow 0$) emission over the inner wings, and integration of the CO ($J = 2 \rightarrow 1$) emission over the outer wings (where ^{13}CO is not observable). Total mass, momentum rate, and mechanical luminosity of the outflow gas are the sum of the parameters given in columns 7, 8, and 9, respectively

[b] LSR velocity range used in the integration of the high-velocity wings of the CO and ^{13}CO lines

[c] Integrated intensity of the CO and ^{13}CO lines over the velocity range given in column 1

[d] Maximum value for the optical depth in the CO and ^{13}CO high-velocity wings, obtained from the radiative transfer equation, assuming the same excitation temperature as that obtained from the CO line center, $T_{ex} = 19$ K (see Sect. 2.2). A filling factor of unity has also been assumed

[e] CO and ^{13}CO column densities of the high velocity gas, obtained from $[N(CO)/cm^{-2}] = 5.15\ 10^{14}\ [\tau/(1 - e^{-\tau})]\ [\int T_R^* dv/K\ km\ s^{-1}]$, and $[N(^{13}CO)/cm^{-2}] = 1.26\ 10^{15}\ [\tau/(1 - e^{-\tau})]\ [\int T_R^* dv/K\ km\ s^{-1}]$, for $T_{ex} = 19$ K. We have adopted the opacities given in column 3

[f] Molecular hydrogen column density, obtained from column 4, assuming abundances $[CO/H_2] = 1.8\ 10^{-4}$ and $[^{13}CO/H_2] = 2\ 10^{-6}$ (Dickmann 1978)

[g] FWHM of the wing integrated intensity map

[h] Mass of the outflow obtained from column 5. An area of πr^2, where $r = \frac{1}{2}(l_a \times l_b)^{1/2}$, has been adopted

[i] Momentum rate of the molecular outflow = MV^2/R. R is $(l_a \times l_b)^{1/2}$, while V is the highest relative velocity at which wing emission has been observed in each velocity range of integration given in column 1 (i.e., 20, 6, 6, and 25 km s^{-1} respectively)

[j] Mechanical luminosity = $MV^3/2R$

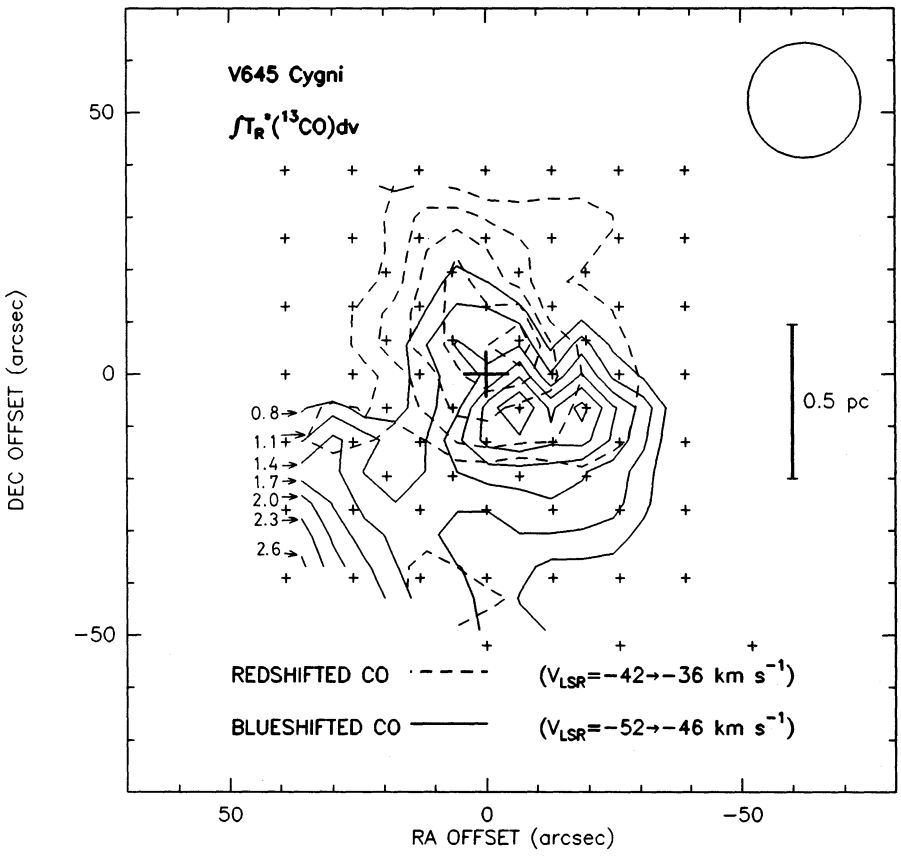

Fig. 6. Contour map of the integrated intensity of the ^{13}CO ($J = 1 \rightarrow 0$) line wings over the velocity ranges from −52 to −46 km s^{-1} (blueshifted gas) and from −42 to −36 km s^{-1} (redshifted gas). Lowest contour levels are 0.8 K km s^{-1} with increment steps of 0.3 K km s^{-1} (blueshifted emission) and 0.5 K km s^{-1} (redshifted emission)

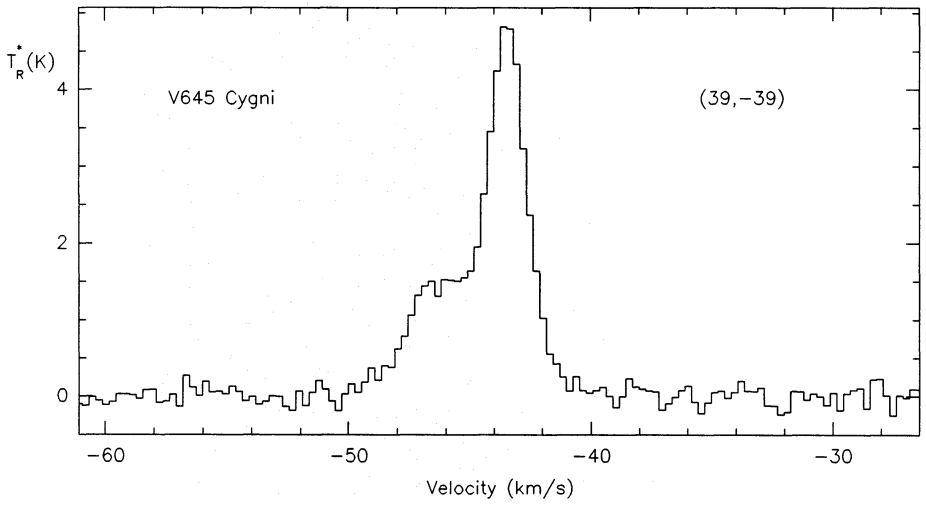

Fig. 7 Observed $^{13}CO\,(J=1\rightarrow0)$ spectrum toward the (39″, −39″) position

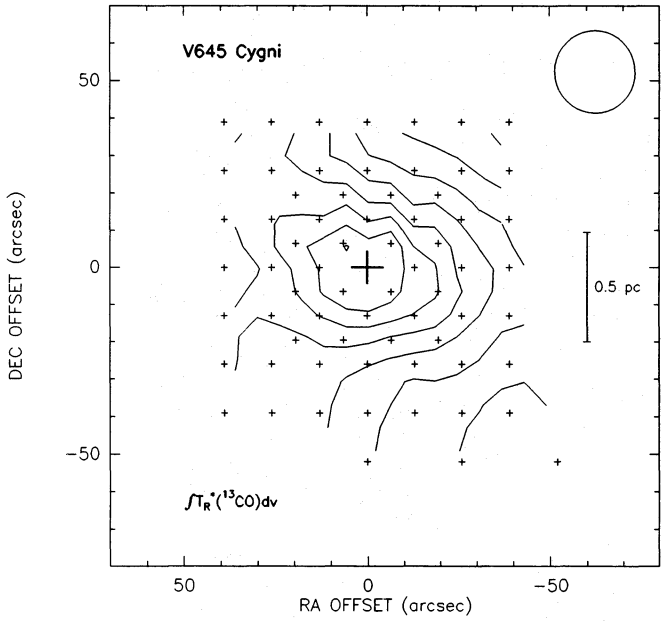

Fig. 8. Contour map of the integrated intensity of the $^{13}CO\,(J=1\rightarrow0)$ line over a velocity range from −50 to −38 km s^{-1}. Contour levels are 3, 6, 9, 12, 15, 18, 21, and 24 K km s^{-1}

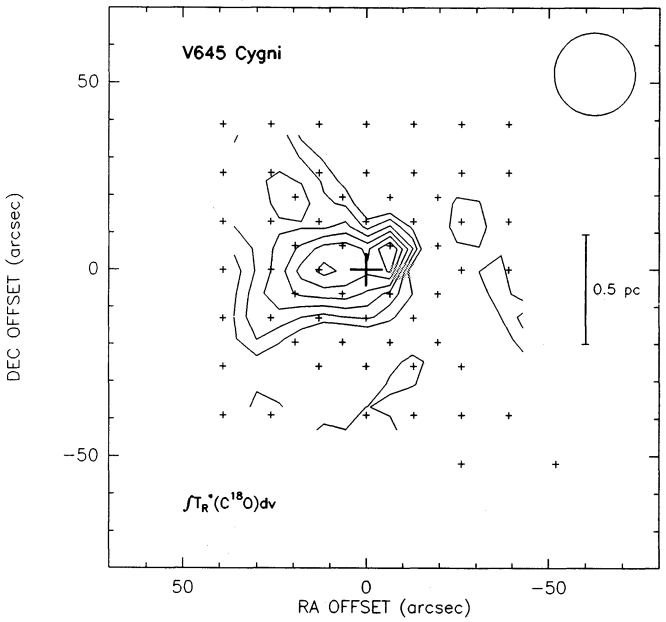

Fig. 9. Contour map of the integrated intensity of the $C^{18}O\,(J=1\rightarrow0)$ line over a velocity range from −50 to −38 km s^{-1}. Contour levels are 1.5, 2, 2.5, 3, 3.5, and 4 K km s^{-1}

Moriarty-Shieven & Snell 1988). On the other hand, an observed decelerating outflow would imply a wind acceleration relatively close to the stellar surface. Later, this stellar wind will suffer a deceleration through interaction with the ambient molecular gas.

A decelerating molecular outflow? (1) As discussed above, the V645 Cyg molecular outflow may be driven by radiation pressure. Radiatively driven wind models (see, e.g., Barlow & Cohen 1977) predict a stellar wind acceleration up to a few stellar radii. Consistent with that, Hamann & Persson (1989) have found that the V645 Cyg stellar wind is accelerated at less than 0.15 AU $\simeq 4\ 10^{-5}$ arcsec ($\sim$5 stellar radii) from the star. The resulting molecular outflow, observable beyond this distance, is expected to exhibit a decelerating pattern by interaction with the ambient molecular cloud.

(2) As it has already been outlined, the spatial distribution of the centroid positions of the high-velocity emission as a function of velocity shows that the angular separation between the redshifted and blueshifted CO lobes is higher at lower relative velocities, which is suggestive of a decelerating pattern for the velocity field (see Fig. 4). Individually, the blueshifted lobes show a decelerating pattern from the central position up to $\sim$16″ south. The redshifted lobes span over a wider range of velocities and exhibit a more complicated behavior with respect to the (0,0) position: at moderate relative velocities ($\leq$10 km s^{-1}) the centroid positions

Table 3. Parameters of the ambient molecular cloud

$T_R^*(^{13}CO)$[a] (K)	$T_R^*(C^{18}O)$[a] (K)	τ_{13}[b]	τ_{18}[b]	$\int T_R^*(^{13}CO)\,dv$[c] (K km s^{-1})	$\int T_R^*(C^{18}O)\,dv$[c] (K km s^{-1})	$N(^{13}CO)$[d] (10^{16} cm^{-2})	$N(C^{18}O)$[d] (10^{15} cm^{-2})	$[^{13}CO/C^{18}O]$[e]	$N(H_2)$[f] (10^{22} cm^{-2})	$l_a \times l_b$[g] (pc)	M[h] ($M_\odot$)	A_V[i] (mag)
7.8	1.3	0.7	0.09	24.5	4.2	4.3	5.5	8	2.1	$\geq 1.1 \times 0.5$	≥ 140	21

[a] Peak line intensity toward the integrated intensity maximum.
[b] Optical depth derived from the transfer equation, assuming $T_{ex}(^{13}CO) = T_{ex}(C^{18}O) = T_{ex}(CO) = 19$ K (see Sect. 2.2), and a filling factor of unity.
[c] Integrated intensity over the range $-50 \leq V_{LSR} \leq -38$ km s^{-1}.
[d] Column density obtained from $[N/cm^{-2}] = 1.26\ 10^{15}\ [\tau/(1-e^{-\tau})]\ [\int T_R^*\,dv/K\ km\ s^{-1}]$, for $T_{ex} = 19$ K.
[e] Abundance ratio obtained from τ_{13}/τ_{18}.
[f] Molecular hydrogen column density obtained from $N(C^{18}O)$ and assuming abundances $[^{13}CO/C^{18}O] = 8$ (this paper) and $[^{13}CO/H_2] = 2\ 10^{-6}$ (Dickman 1978).
[g] FWHM of the $C^{18}O$ emission.
[h] Mass of the ambient clump. An area of πr^2, where $r = \frac{1}{2}(l_a \times l_b)^{1/2}$, has been adopted.
[i] Visual extinction, from $[A_V/mag] = 10 \times [N(H_2)/10^{22}\ cm^{-2}]$ (Spitzer 1978).

are located to the north of the (0,0) position (see Fig. 4) with the larger separations found for the lower relative velocities. This is also suggestive of deceleration. However, at high relative velocities (≥ 10 km s^{-1}) the centroids are located to the south of the (0,0) position. We think that this peculiar behavior of the red lobe centroids, with the moderate velocity centroids located to the north and the highest velocity centroids to the south, could be a result of projection effects as we will discuss in what follows.

For an axis-symmetrical bipolar outflow with its axis tilted with respect to the line-of-sight, points that are symmetric with respect to the outflow axis have the same *true* velocity, but the projected velocity along the line-of-sight (*observed* velocity) is different. Let us consider the red lobe of a decelerating outflow, tilted as in Fig. 11a (red lobe to the north). As the outflow is decelerating, the maximum true velocity occurs near the exciting source, where the projected velocity is higher for points under the outflow axis than above it, due to the opening angle of the outflow. We give the quantitative results for specific values of the geometrical parameters in the case of a layer of flowing gas with biconical geometry (Fig. 11). The graph shows the distance p to the z-axis as a function of the line-of-sight velocity (V_z) for points in the z-p plane. The broken line corresponds to the portion of the red lobe located above the symmetry axis of the outflow, and the solid line, to the portion under the symmetry axis. Note that the highest projected velocities appear only to the south of the z-axis ($p < 0$), while the low velocities tend to appear to the north ($p > 0$), where the bulk of the red lobe is located. This will produce a shift of the red lobe emission centroids from north to south, as the line-of-sight velocity increases. The qualitative results outlined are essentially independent of the specific parameters adopted for the model. Similar qualitative results are also obtained with a bi-ellipsoidal geometry.

We emphasize that these results are only obtained from geometrical considerations, and thus, they cannot be used to predict detailed maps of the observed emission. However, it is worth noting that these results suggest that our data on the V645 Cyg outflow are in agreement with what should be expected from a decelerating outflow with its axis seen nearly "pole-on". That is, the red and blue lobes appear slightly separated in the north-south direction, and this separation increases as the relative velocity decreases; the redshifted emission at low relative velocities appears centered to the north of the exciting source, but at high velocities, this emission appears displaced to the south of the exciting source. A symmetrical behavior should be expected for the blueshifted emission. However, the poorer signal-to-noise ratio in the blue wing emission does not allow us to establish the behavior of the high velocity blueshifted gas.

Collimation? The fact that the ambient molecular cloud in the inner region appears perpendicular to the north-south optical (Goodrich 1986; Lenzen 1987) and molecular outflow (this paper), together with the east-west velocity gradient observed in ^{13}CO and $C^{18}O$ (Fig. 10), could suggest the presence of a rotating disk-like structure related to the north-south collimation process. Indeed, the inferred mass from the $C^{18}O$ observations (Table 3) is sufficient to bind these east-west motions. We must note that the presence of an even smaller circumstellar east-west disk-like structure around V645 Cyg has been proposed by Hamann & Persson (1989) to explain the observed optical and near infrared line profiles. Disks or toroids inside disks or toroids have been found in other sources (see Rodríguez 1988). The change of orientation of the molecular outflow from a north-south to a southeast-northwest direction for scales $\geq 1'$ could be explained if the molecular outflow is deflected by the outer parts of the molecular cloud.

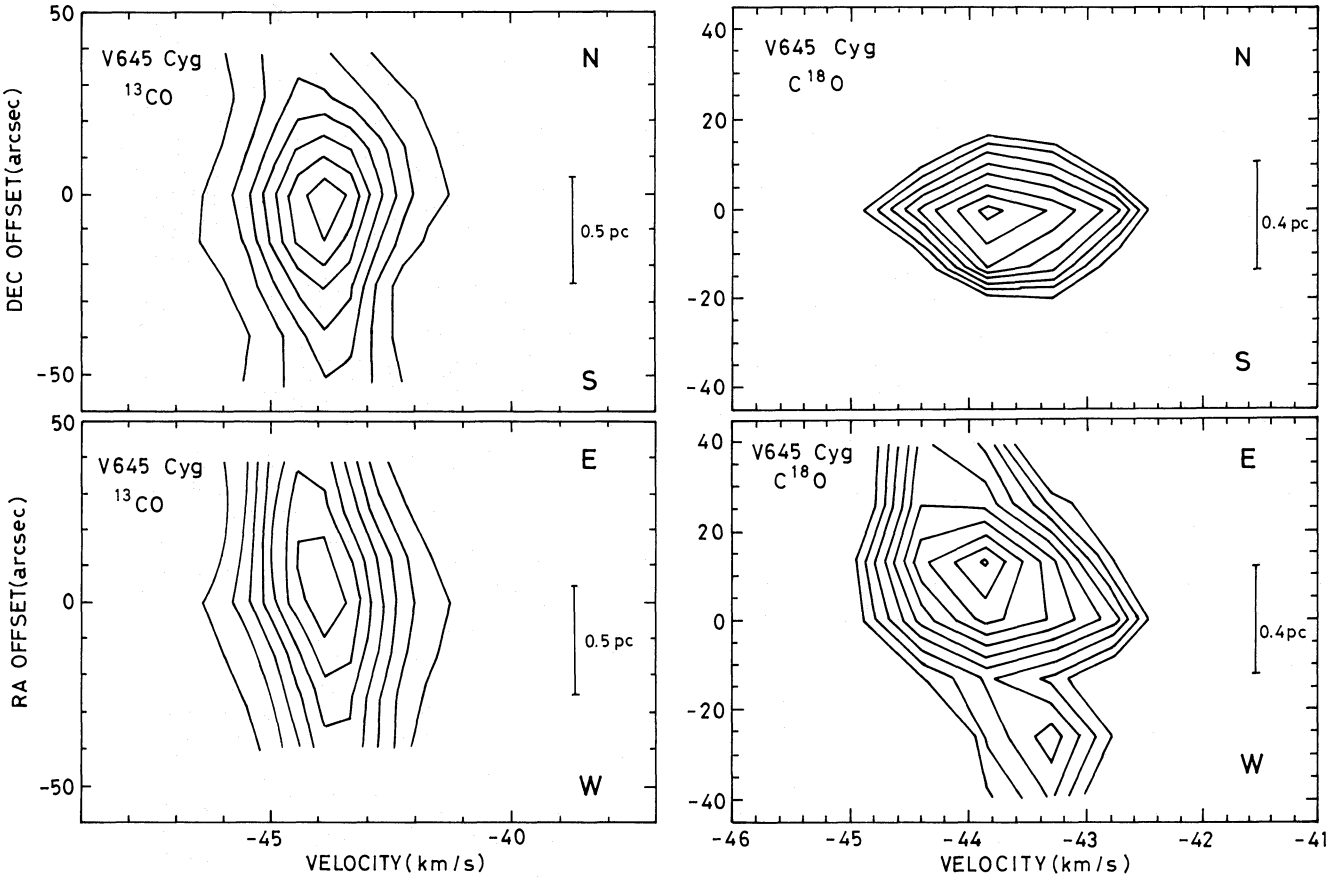

Fig. 10. Position velocity diagrams for the ^{13}CO ($J=1\rightarrow0$) (*left*) and $C^{18}O$ ($J=1\rightarrow0$) (*right*) along the north-south (*top*) and east-west (*bottom*) directions through the (0,0) position. Lowest contours are 1 K (^{13}CO) and 0.7 K ($C^{18}O$) with increment steps of 1 K (^{13}CO) and 0.1 K ($C^{18}O$)

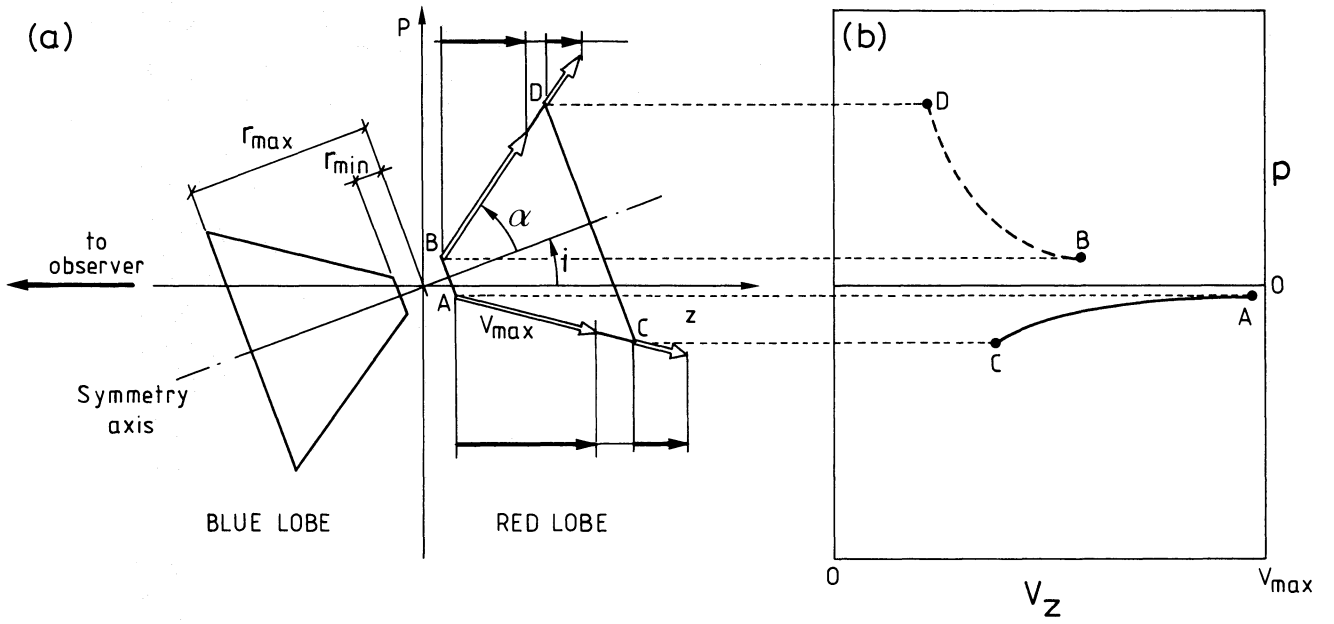

Fig. 11. **a** Schematic representation of a biconical layer of decelerating outflowing gas. The plane of the figure is the plane defined by the line of sight and the outflow axis. Note that symmetrical points, with respect to the outflow axis, do not have the same line-of-sight velocity: points under the outflow axis have higher projected velocities than points above the outflow axis. **b** Distance to the z-axis (p) as a function of the line-of-sight velocity (V_z) for points in the z-p plane. The solid line corresponds to the points under the symmetry axis of the outflow and the broken line corresponds to the points above this axis. The parameters adopted for the model are: $i=20°$, $\alpha=35°$, $V/V_{max}=(r/r_{min})^{-0.5}$

4. Conclusions

Using the IRAM 30-m telescope, we have observed the CO ($J=2\rightarrow1$), ^{13}CO ($J=1\rightarrow0$), and $C^{18}O$ ($J=1\rightarrow0$) rotational transition lines toward the V645 Cyg (AFGL 2789) region. Our main conclusions are the following:

(1) The physical parameters obtained for the V645 Cyg outflow are lower than for other outflows with exciting sources of similar luminosity ($L_* \simeq 10^4\ L_\odot$). In particular, the derived momentum rate in the outflow is similar to the momentum rate in the radiation field of the star, allowing that a *classical* mechanism such as the radiation pressure could be driving the outflowing gas.

(2) The spatial distribution of the CO wing emission corroborates the north-south bipolarity of the V645 Cygni outflow at small scales. This bipolarity is more apparent at low relative velocities, while at higher relative velocities the outflow seems isotropic.

(3) The behavior of the CO wing emission at different velocities, suggests, at the observed scale, a decelerating pattern for the outflowing molecular gas.

(4) The observed ^{13}CO spectra exhibit high-velocity wing emission with a bipolar distribution similar to that observed in CO in the central region. A significant enhancement of the ^{13}CO blueshifted emission appears to the southeast corner of our mapped region. This fact suggests that, at larger scales, the outflow axis could be close to the southeast-northwest direction, as found by other authors.

(5) We have found an elongated $C^{18}O$ structure with a velocity gradient of $\sim 0.7\,km\,s^{-1}\,pc^{-1}$ in the east-west direction. These motions may be bound by the observed molecular mass.

Acknowledgements. We would like to thank an anonymous referee for helpful comments. We acknowledge the hospitality offered by the IRAM (Granada, Spain) where part of the data reduction was made. The authors are partially supported by SEUI (Spain) Grant PB87-0371. JFG, JMT and LV are partially supported by Junta de Andalucía (Spain). GA is in receipt of a fellowship from Direcció General d'Universitats and CIRIT de Catalunya (Spain).

References

Anglada G., Rodríguez L. F., Cantó J., Estalella R., López R., 1987, A&A 186, 280
Bally J., Lada C. J., 1983, ApJ 265, 824
Barlow M. J., Cohen M., 1977, ApJ 213, 737
Cabrit S., Bertout C., 1986, ApJ 307, 313
Cohen M., 1977, ApJ 215, 533
Curiel S., Rodríguez L. F., Cantó J., Bohigas J., Roth M., Torrelles J. M., 1989, Astron. Lett. Comm. 27, 299
Dickman R. L., 1978, ApJS 37, 407
Dyson J. E., 1984, Ap&SS 106, 181
Goodrich R. W., 1986, ApJ 311, 882
Hamann F., Persson S. E., 1989, ApJ 339, 1078
Herbig G. H., 1968, ApJ 152, 439
Kutner M. L., Ulich B. L., 1981, ApJ 250, 341
Lada C. J., 1985, ARA&A 23, 267
Lada C. J., Blitz L., Reid M. J., Moran J. M., 1981, ApJ 243, 769
Lenzen R., 1987, A&A 173, 124
Moriarty-Shieven G. H., Snell R. L., 1988, ApJ 332, 364
Morris M., Kazès I., 1982, A&A 111, 239
Pudritz R. E., Norman C. A., 1986, ApJ 301, 571
Rodríguez L. F., 1988, in: Galactic and Extragalactic Star Formation, eds. R. E. Pudritz and M. Fich, Kluwer, Dordrecht
Rodríguez L. F., 1989, Rev. Mexicana Astron. Astrof. 18, 45
Rodríguez L. F., Carral P., Ho P. T. P., Moran J.M., 1982, ApJ 260, 635
Rodríguez L. F., Torrelles J. M., Moran J. M., 1981, ApJ 86, 1245
Schulz A., Black J. H., Lada C. J., Ulich B. L., Martin R. N., Snell R. L., Erickson N. J., 1989, ApJ 341, 288
Spitzer L., 1978, Physical Processes in the Interstellar Medium, John Wiley, New York
Torrelles J. M., 1990, PASPC (in press)
Torrelles J. M., Anglada G., Rodríguez L. F., Cantó J., Barral J. F., 1987, A&A 177, 171
Torrelles J. M., Ho P. T. P., Rodríguez L. F., Cantó J., Verdes-Montenegro L., 1989, ApJ 346, 756
Torrelles J. M., Rodríguez L. F., Cantó J., Carral P., Marcaide J., Moran J. M., Ho P. T. P., 1983, ApJ 274, 214
Uchida Y., Shibata K., 1985, PASJ 37, 315